NACE® INTERNATIONAL

CORROSION 2016
CONFERENCE & EXPO

Effect of Incorporation of Calcium into Iron Carbonate Protective Layers in CO_2 Corrosion of Mild Steel

Saba Navabzadeh Esmaeely, David Young, Bruce Brown and Srdjan Nešić

Institute for Corrosion and Multiphase Technology

Department of Chemical and Biomolecular Engineering

Ohio University, Athens, OH 45701

ABSTRACT

In aqueous carbon dioxide (CO_2) solutions where both Ca^{2+} and ferrous iron (Fe^{2+}) are present, such as downhole gas reservoirs or deep saline aquifers after CO_2 injection, mixed metal carbonates with the formula $Fe_xCa_yCO_3$ ($x+y$=1) can form. This inhomogeneity may lead to localized corrosion. During carbon steel corrosion experiments conducted in electrolytes containing high Ca^{2+} concentrations, inhomogeneous corrosion product layers with the composition $Fe_xCa_yCO_3$ ($x+y$=1) were indeed observed, along with non-uniform corrosion. Determining relative molar fractions of Ca^{2+} and Fe^{2+} in $Fe_xCa_yCO_3$ is paramount to predicting the relative properties and stability of such mixed metal carbonates. Using Bragg's Law and equations to relate inter-planar spacings to unit cell parameters, X-ray diffraction (XRD) data yielded values for the molar fraction of Ca^{2+} in $Fe_xCa_yCO_3$. Procedures in the current experimental study were designed to develop a range of specific corrosion product layers on mild steel samples. Experiments were conducted at constant Cl^- concentration with and without 10,000 ppm Ca^{2+} in stagnant conditions, for two different flow conditions. In stagnant conditions, localized corrosion was associated with the presence of Ca^{2+} and the inhomogeneity of the corrosion product layer. The corrosion attack became uniform when flow was introduced.

Key words: calcium; CO_2 corrosion; $CaCO_3$; $FeCO_3$; $Fe_xCa_yCO_3$; flow; localized corrosion, XRD.

INTRODUCTION

The effect of calcium cations (Ca^{2+}) on the formation and protectiveness of iron carbonate ($FeCO_3$) layers in aqueous carbon dioxide (CO_2) corrosion of mild steel was discussed in a previous study.[1] It

showed that the isostructurality of calcium carbonate ($CaCO_3$) and $FeCO_3$ allowed the incorporation of Ca^{2+} into the $FeCO_3$ structure; thus, the morphology and chemical properties of $FeCO_3$ were altered.

The importance of $FeCO_3$ formation on corrosion protection of mild steel has been well documented.[2-7] In a stagnant aqueous CO_2 solution, the water chemistry at the corroding steel surface is not the same as the bulk water chemistry. As a consequence of the corrosion process that consumes hydrogen (H^+) and releases ferrous iron (Fe^{2+}) to the solution, the pH and Fe^{2+} concentration increase adjacent to the steel surface. This leads to a higher degree of $FeCO_3$ saturation near the steel surface and a higher probability of protective $FeCO_3$ layer formation. However, in a turbulent well-mixed solution a corroding bare steel surface has almost the same water chemistry as the bulk solution, making protective $FeCO_3$ layer formation less probable.[2,6-9] In addition, at very high flow rates, there is a possibility of removal of protective $FeCO_3$ layers, leading to localized corrosion.[8,9]

The effect of Ca^{2+} in CO_2 corrosion of mild steel has been generally underestimated, and there is little consistent data reported. For example, Jiang, et al.,[10] reported localized corrosion in CO_2 solutions containing calcium chloride ($CaCl_2$) and claimed that chloride ions (Cl^-) caused localized corrosion while Ca^{2+} delayed the initiation process, however, due to short experiments it was not clear whether pit propagation was affected the same way. Ren, et al.,[11] and Zhu, et al.,[12] observed localized corrosion in CO_2 solutions containing $CaCl_2$ and also stated that this was due to the presence of Cl^-, even if the experimental evidence did not allow them to distinguish the effect of Cl^- from that of Ca^{2+}. On the other hand, Gao, et al.,[13] reported that formation of "mixed" metal carbonates ($Fe_xCa_yCO_3$ and $Fe_x(Mg,Ca)_yCO_3$ where $x + y = 1$) in the precipitated layers was responsible for localized corrosion. From this brief literature review, it remains unclear what mechanism is responsible for localized corrosion due to of $CaCl_2$ presence in aqueous CO_2 solutions.

Therefore, the following questions are addressed in the present study:

1. Is it Cl^- or Ca^{2+} that leads to localized corrosion of mild steel in CO_2 solutions?
2. What is the effect of flow on the protectiveness of the precipitated $Fe_xCa_yCO_3$ layer?
3. What is the exact composition of the $Fe_xCa_yCO_3$ layers precipitated on the mild steel surface and how is it related to corrosion?

EXPERIMENTAL PROCEDURE

The test matrix is shown in .14
Table 1. A conventional 2 L glass cell with a three-electrode electrochemical setup, was used and the procedure was the same as described in the previous study conducted by Esmaeely, et al.[1] The main

difference is related to the use of a magnetic stirrer to simulate flowing conditions in the glass cell. The desired Ca^{2+} concentration was obtained by addition of $CaCl_2$. In order to have 10,000 ppm Ca^{2+} in the bulk solution, 54.7 g $CaCl_2$ was added to the cell. This also meant that 17,800 ppm Cl^- was present in the bulk solution, which raised concerns that this concentration would affect corrosion rate, rather than Ca^{2+}. Therefore, a "baseline" experiment was also conducted with the same amount of Cl^-, but with no Ca^{2+} in the solution (in this case the Cl^- concentration was achieved by adding NaCl). A potentiostat was used to monitor the open-circuit potential (OCP); corrosion rate was measured using the linear polarization resistance (LPR) method. Surface analyses were performed using X-ray diffraction (XRD; $CuK\alpha$), scanning electron microscopy (SEM), energy-dispersive X-ray spectroscopy (EDS), and profilometry. Inductively coupled plasma (ICP) spectroscopy was used to measure the Ca^{2+} concentration in samples of the aqueous solution. The Fe^{2+} concentration was measured by spectrophotometry. To reveal the steel surface underneath the corrosion product layer, a Clarke solution treatment was performed on one sample from each experiment, following the ASTM [1] G1 standard guidelines to remove the corrosion product layer.[14]

Table 1

Test Matrix

Parameters	Experiment 1 (baseline)	Experiment 2	Experiment 3	Experiment 4
Total pressure	0.1 MPa	0.1 MPa	0.1 MPa	0.1 MPa
pCO_2	0.05 MPa	0.05 MPa	0.05 MPa	0.05 MPa
Temperature	80°C	80°C	80°C	80°C
NaCl	4 wt.%	1 wt.%	1 wt.%	1 wt.%
Ca^{2+}	0	10,000 ppm	10,000 ppm	10,000 ppm
Initial pH	5.5	5.3	5.5	5.5
Flow	stagnant	Stagnant	300 rpm	600 rpm
Steel	UNS[2] G10180	UNS G10180	UNS G10180	UNS G10180

*Ca^{2+} added as $CaCl_2$

⌀ a magnetic stirrer was used for solution agitation

---

[1] American Society for Testing and Materials, 100 Barr Harbor Drive, PO Box C700, West Conshohocken, PA, 19428-2959 | USA

[2] UNS numbers are listed in Metals and Alloys in the Unified Numbering System, published by the Society of Automotive Engineers (SAE International) and cosponsored by ASTM International.

RESULTS

Figure 1 shows the evolution of corrosion rate over time for each test condition. In all experiments, the corrosion rate decreased over time as shown in Figure 1. For two experimental conditions the corrosion rate decreased and stabilized at approximately 1 mm/yr. This could be due to formation of a partially protective layer. In the other two experiments, the corrosion rate decreased to less than 0.2 mm/yr. In those experiments a protective layer likely formed on the steel surface.[6,15,16] In two of the four conditions the experiments were repeated with very similar results.

Based on the previous study conducted by Esmaeely, *et al.*,[1] it was suspected that even when low general corrosion rates were detected by LPR, indicating a formation of a "protective layer", there was a possibility of localized corrosion, which needed to be investigated. There, it was suggested that due to partial substitution of Fe^{2+} in the $FeCO_3$ lattice by Ca^{2+} and vice versa, a mixed iron/calcium carbonate forms on the steel surface.[1,17] This mixed carbonate layer is apparently not as protective as a pure $FeCO_3$ layer. This issue is further explored in the last section of this paper.
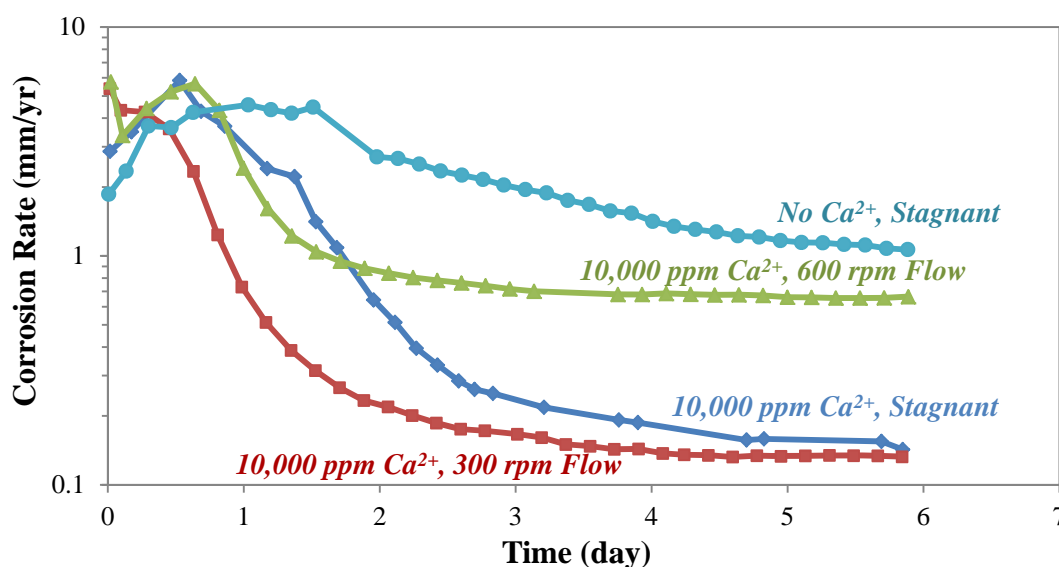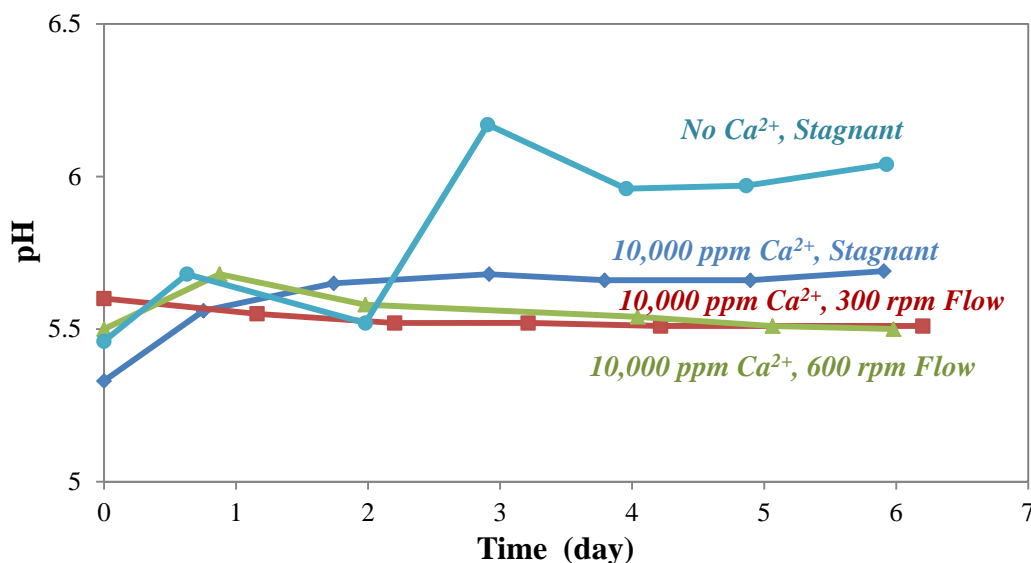

Figure 1: Evolution of corrosion rate for mild steel exposed to a simulated brine solution with equal Cl⁻ concentrations with and without Ca^{2+} at different flow velocities at 80°C and pCO_2 of 0.05 MPa.

When steel corrodes in an aqueous CO_2 solution, it will typically lead to an increase of pH due to accumulation of corrosion products (increased Fe^{2+} concentration). This is particularly true when steel-surface-to-solution-volume ratio is high, as was the case in the glass cell experiments presented here. Figure 2 shows that the pH for the baseline experiment (with no Ca^{2+}) was constant for 2 days due to periodical injections of deoxygenated diluted hydrochloric acid, which were done in order to maintain a stable pH. When the injections were stopped after 2 days, the pH increased as expected, making the solution supersaturated with respect to $FeCO_3$. The supersaturation leads to precipitation of solid

$FeCO_3$, and to solution acidification.[1] When the two processes achieve a balance (Fe^{2+} production by corrosion and Fe^{2+} depletion by precipitation) a stable pH is obtained as seen in Figure 2.

Experiments that contained 10,000 ppm Ca^{2+} stayed stable at the initial pH 5.5, without any pH adjustment. This was because of the equilibrium for $CaCO_3$ (which was targeted at pH5.5) was spontaneously maintained throughout the experiment. Therefore no significant precipitation of $CaCO_3$ was expected and consequently no solid $CaCO_3$ formation was visible in the glass cell. Since the concentration of Ca^{2+} was many orders of magnitude higher than that of Fe^{2+}, and the solubility of $CaCO_3$ was lower than that of $FeCO_3$, the pH was spontaneously maintained at the $CaCO_3$ equilibrium.

Figure 2: Variation of pH for a simulated brine solution with equal Cl⁻ concentrations with and without Ca^{2+} at different flow velocity at 80°C and pCO_2 of 0.05 MPa.

Figure 3 shows the SEM images of steel samples from each experiment after 6 days. The SEM images for the steel sample exposed to the baseline conditions (no Ca^{2+}) is shown in Figure 3 to be partially covered by $FeCO_3$ crystals. The sample exposed to 10,000 ppm Ca^{2+}, Figure 3 (b), shows that the surface was not uniformly covered by the corrosion product or scale layer. The corrosion product or scale layer on the samples retrieved from experiments with Ca^{2+} and different flow conditions are shown in Figure 3 (c) and (d). No significant differences were observed between these samples.

In order to determine compositional analysis of the layer on the samples from solutions containing 10,000 ppm Ca^{2+}, XRD analysis was performed on each. The results are shown in Figure 4. The most intense Bragg reflection for both $CaCO_3$ and $FeCO_3$ corresponds to the (104) inter-planar d-spacing, within their Bravais lattices, located at 29.42 2Θ and 32.07 2Θ, respectively.[20] In each of the X-ray

diffraction patterns the (104) peak is shifted to a higher 2Θ value, and is consistent with substitution of Ca^{2+} with the smaller Fe^{2+} into equivalent lattice positions.
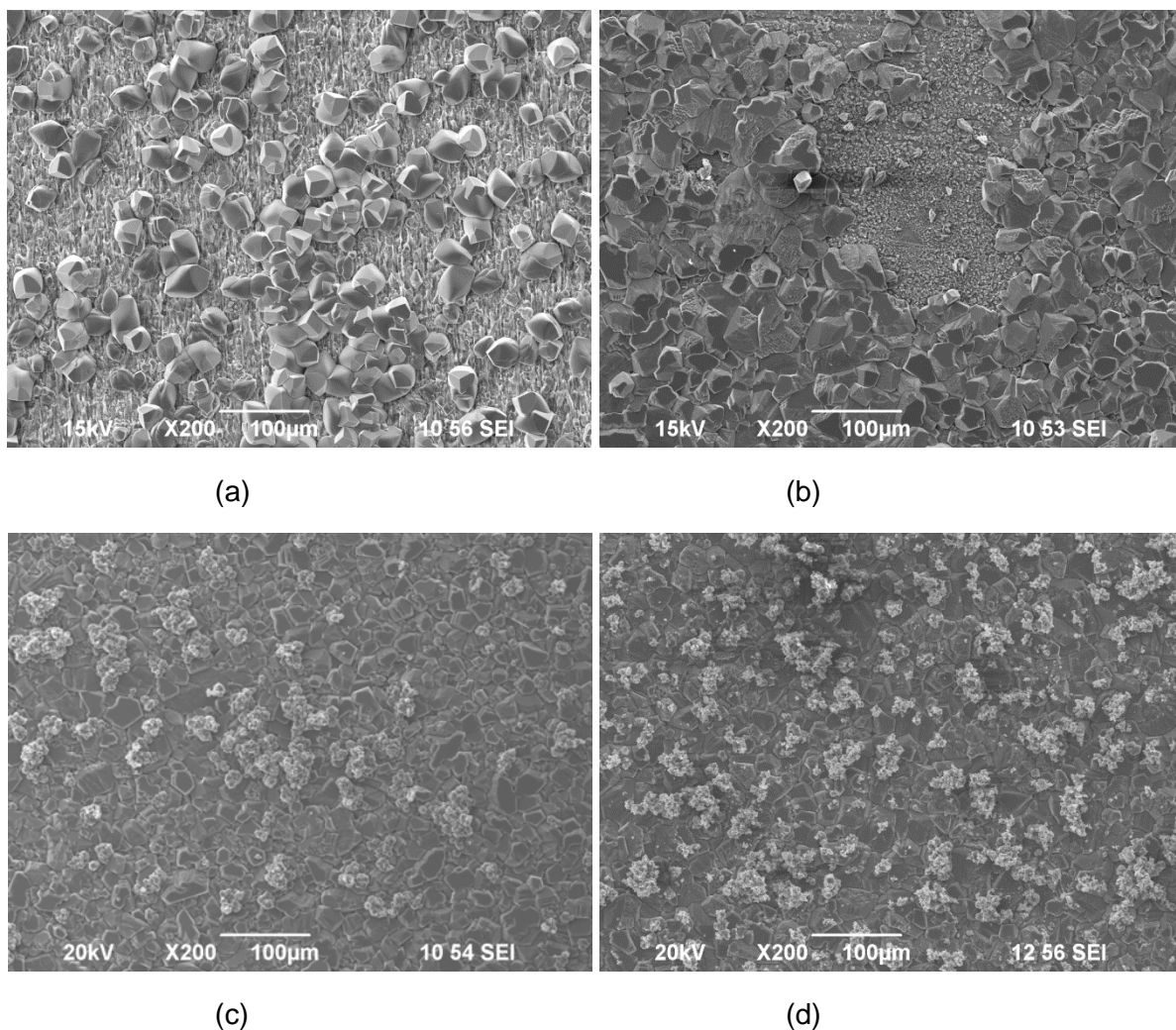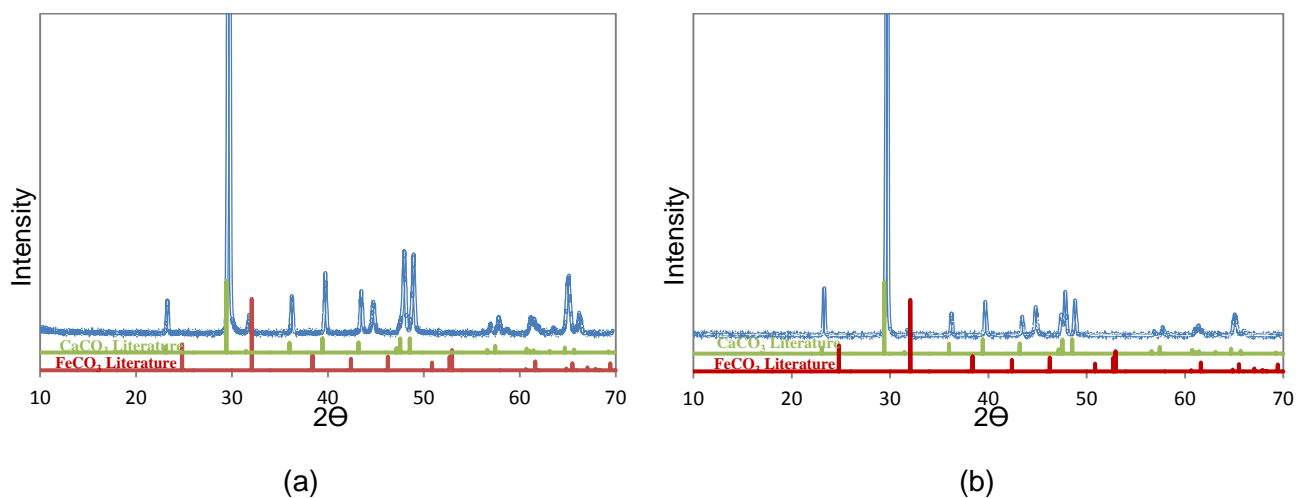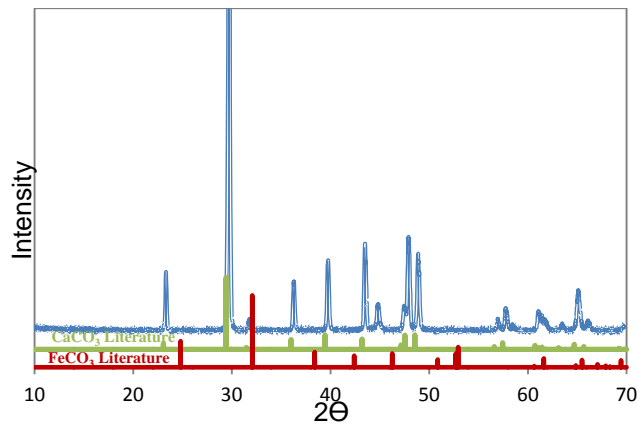

Figure 3:SEM images of samples (UNS G10180) removed after 6 days exposure to solutions at 80°C and pCO$_2$ of 0.05 MPa with (a) 4 wt% NaCl in stagnant condition; (b) 10,000 ppm Ca^{2+} in stagnant condition; (c) 10,000 ppm Ca^{2+} at 300 rpm; (d) 10,000 ppm Ca^{2+} at 600 rpm.
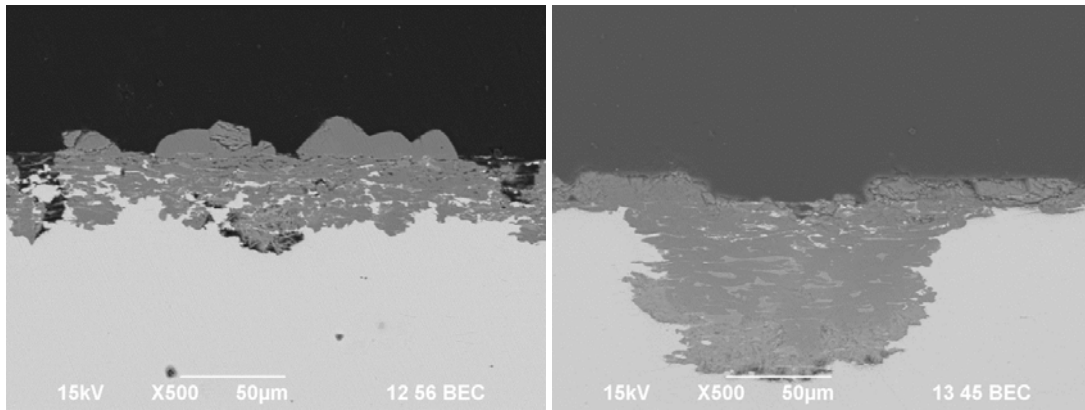
(c)

(c)Figure 4: XRD data of samples (UNS G10180) after 6 days exposure to solutions at 80°C and pCO_2 of 0.05 MPa with (a) 10,000 ppm Ca^{2+} in stagnant condition; (b) 10,000 ppm Ca^{2+} at 300 rpm; (c) 10,000 ppm Ca^{2+} at 600 rpm.

Figure 5 shows the cross-sectional analyses of the samples after 6 days exposure to each test condition. Figure 5 (a) shows a cross-sectioned area for the 4 wt.% NaCl solution. Figure 5 (b) shows the cross-sectioned area of localized corrosion on the sample surface for the experiment with 10,000 ppm Ca^{2+} at stagnant condition. Representative areas for each of the remaining two samples are shown in the cross-sectional images in Figure 5 (c), and (d) for the samples exposed to 10,000 ppm Ca^{2+} at 300 rpm, and 600 rpm respectively. Localized corrosion was investigated further by study of the surface after the corrosion product layer was chemically removed with Clarke Solution.[14]

Figure 6 shows the SEM images of the sample surfaces after removal of the corrosion product or scale layer. Figure 6 (b) and (c) show that the surface of the samples exhibited features that could be consistent with localized corrosion. The surfaces of the samples from the solutions with 4 wt.% NaCl and with 10,000 ppm Ca^{2+} at 600 rpm flow did not reveal any such features. The pit penetration rate is calculated based on the maximum measured pit depth using profilometry, as shown in Figure 8. The pit penetration rates were calculated to be 7.2 mm/yr and 6.2 mm/yr for the experiments with 10,000 ppm Ca^{2+} at stagnant, and at 300 rpm, respectively.
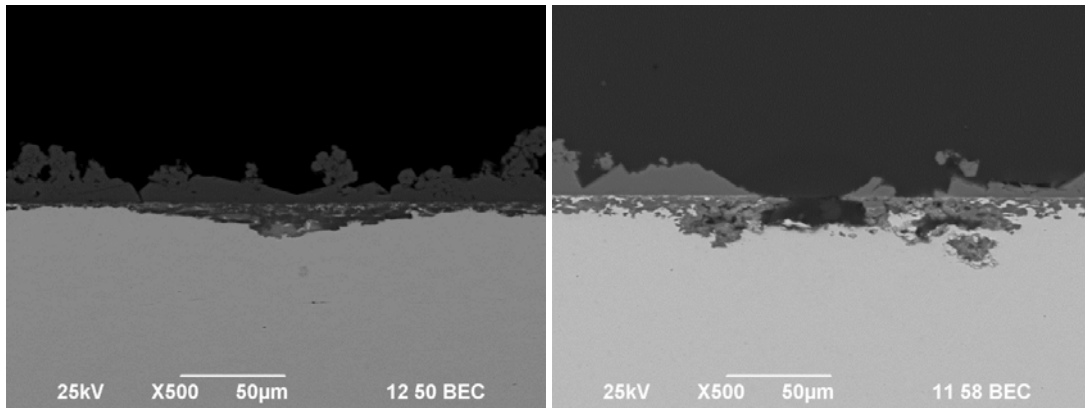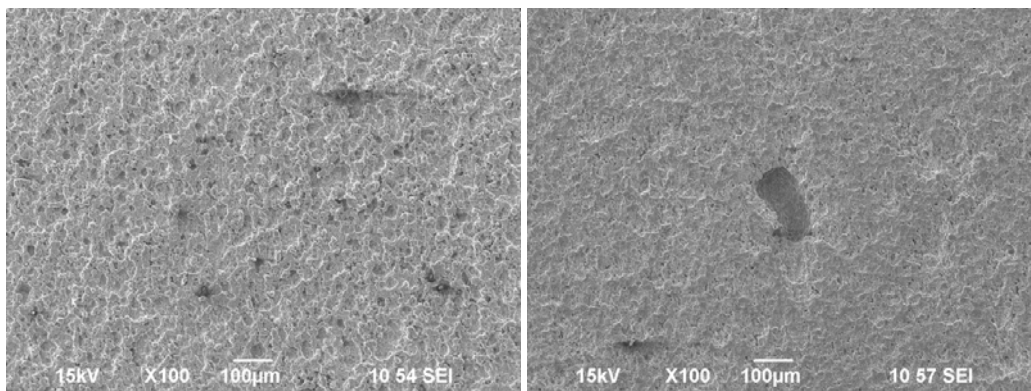
Figure 5: Cross-sectional images of samples (UNS G10180) removed after 6 days exposure to solutions at 80°C and pCO_2 of 0.05 MPa with (a) 4 wt.% NaCl in stagnant condition; (b)10,000 ppm Ca^{2+} in stagnant condition; (c) 10,000 ppm Ca^{2+} at 300 rpm; (d) 10,000 ppm Ca^{2+} at 600 rpm.
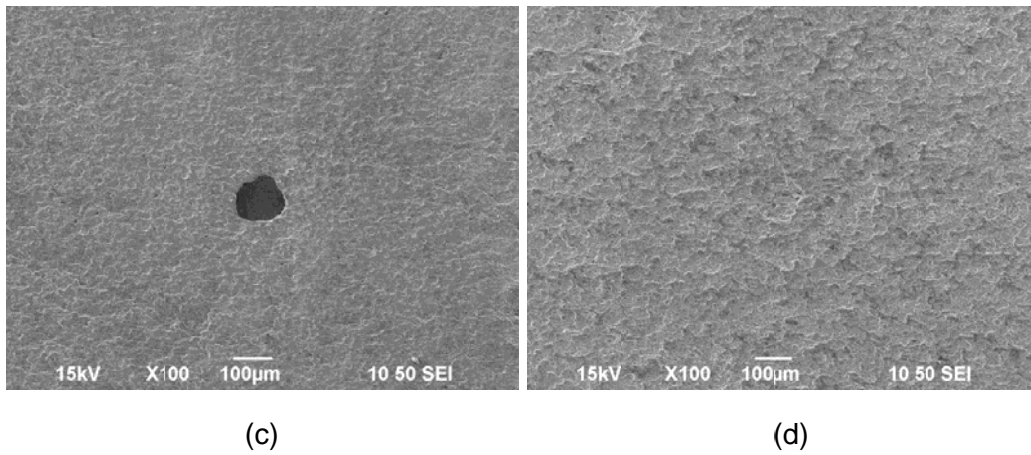
(c)   (d)

Figure 6: Surface after corrosion product removal (UNS G10180) after 6 days exposure to solutions at 80°C and pCO_2 of 0.05 MPa with (a) 4 wt.% NaCl in stagnant condition (b) 10,000 ppm Ca^{2+} in stagnant condition; (c) 10,000 ppm Ca^{2+} at 300 rpm; (d) 10,000 ppm Ca^{2+} at 600 rpm.
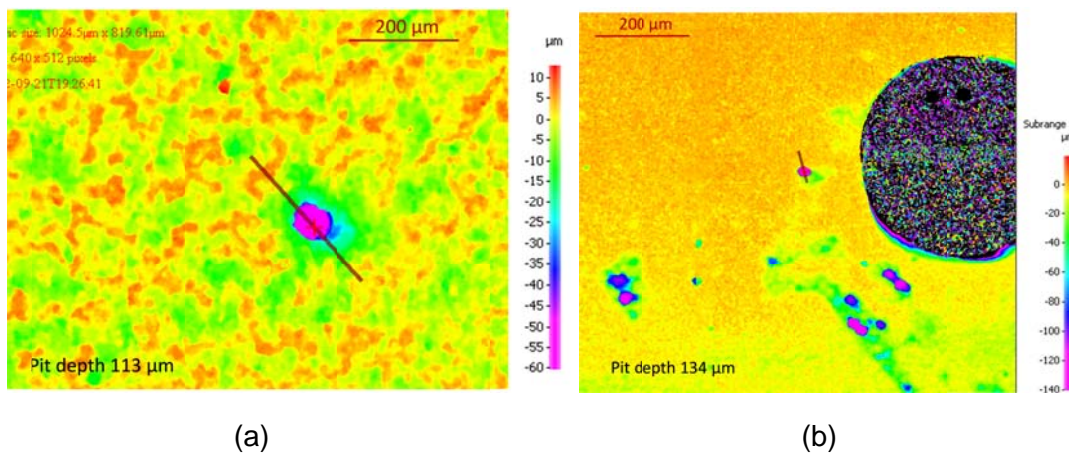

(a)   (b)

Figure 7: Profilometer image of sample (UNS G10180) after removal of corrosion product for the experiment conducted at 80°C and pCO_2 0.05 MPa with (a) 10,000 ppm Ca^{2+} in stagnant condition and (b) 10,000 ppm Ca^{2+} at 300 rpm.

Mole fraction determination of Ca^{2+} in $Ca_xFe_yCO_3$

The XRD data shown in Figure 4 and Figure 9 can be used to calculate the concentration of Ca^{2+} in the lattice structure of the solid solution. Figure 8 shows the hexagonal Bravais Lattice corresponding to the fundamental crystal structure of $FeCO_3$, $CaCO_3$, and $Ca_xFe_yCO_3$ ($x+y=1$), as each phase is isostructural (calcite-type). Unit cell parameters a and c are calculated using Equation (6).[21] Value d in Equation (6) is calculated from Bragg's Law in Equation (7).[21] The a and c unit cell edges are determined using h, k, and l values, or Miller Indices corresponding to particular lattice planes, and the XRD data using d values from Equation (7) . The V unit cell volume can be calculated using a and c. Assuming linear behavior for Ca^{2+} incorporation in the structure versus the unit cell parameters and the unit cell volume,

the mole fraction x of Ca^{2+} in the solid solution $Ca_xFe_yCO_3$ ($x+y=1$) is found using Equation (9).[21] Figure 10 shows the plotted x value versus c for the pure $FeCO_3$ and $CaCO_3$ literature data.[20] The calculated unit cell parameter c for each tested condition is located on the line in Figure 10, and the corresponding mole fraction x of Ca^{2+} is determined. The red points are extracted data from the literature, and confirm the accuracy of the calculated data.[22] The solid triangles are calculated data from the previous study using XRD plots in Figure 9. The open circles are calculated from unit cell parameters in the current study using XRD data from Figure 4. Figure 11 shows the x value versus the unit cell volume. The same procedure was followed to find the x value for each tested condition using the unit cell volume. The same procedure can be used to calculate unit cell parameter a, and to find the corresponding x value, but value a is smaller, and the calculation error is greater on the extracted values. Table 2 shows the results of the calculations. The x value was verified using EDS spectra using the ratio of Ca^{2+} atomic percent to the summation of Fe^{2+} and Ca^{2+} atomic percent. The deviation in the x value using EDS spectra and XRD data are likely related to a Ca^{2+}/Fe^{2+} concentration gradient within the layer on the surface, as was shown in the EDS line scanning in the previous study.[1] The peaks on the XRD plots are asymmetric, which is also indicative of concentration gradients within the solid solution.

$$\frac{1}{d} = \frac{4}{3}\left(\frac{h^2 + hk + k^2}{a^2}\right) + \frac{l^2}{c^2} \tag{1}$$

$$d = \frac{n\lambda}{2\sin\theta} \tag{2}$$

$$V = \frac{\sqrt{3}}{2}a^2 c \tag{3}$$

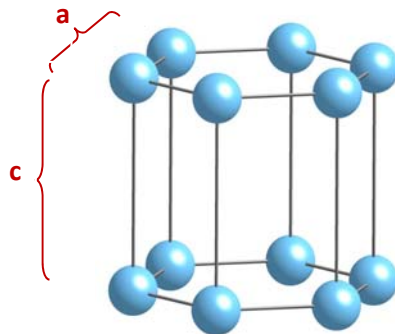$$y = 1.6885\,x + 15.373 \tag{4}$$

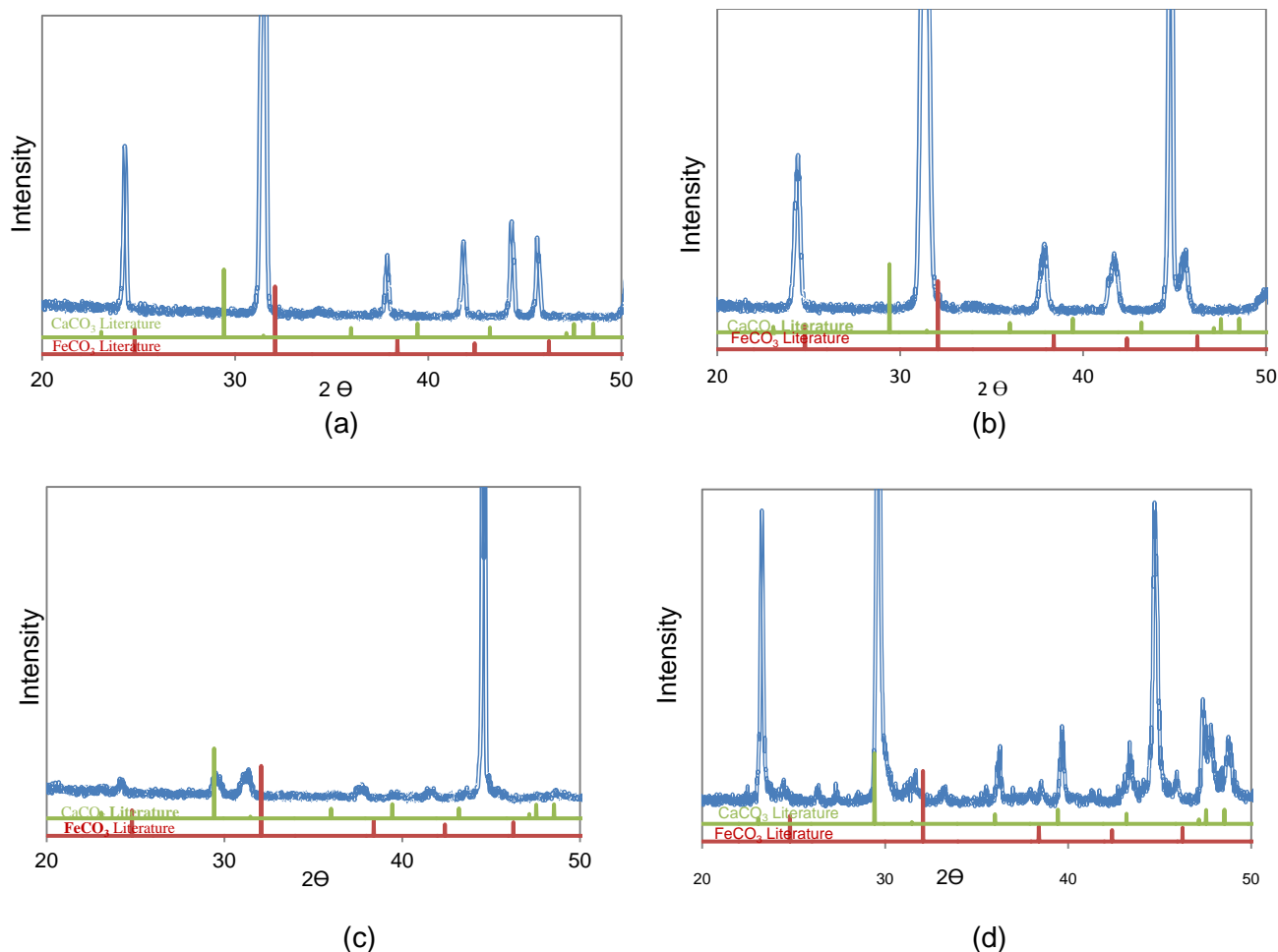**Figure 8: Hexagonal Bravais Lattice**

Figure 9:XRD data of samples (G10180) after 6 days exposure at stagnant condition at 80°C and pCO$_2$ 0.05 MPa with 10 ppm Fe^{2+}, initial pH 6.6. (a) 10 ppm Ca^{2+}; (b) 100 ppm Ca^{2+}; (c) 1000 ppm Ca^{2+}; (d) 10,000 ppm Ca^{2+}[1].
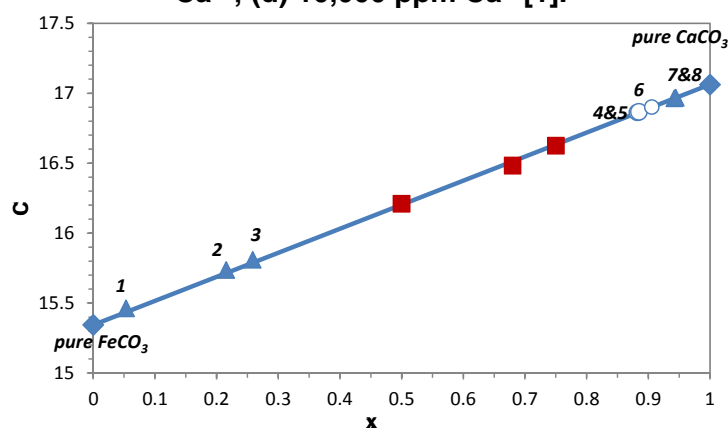

Figure 10: Unit cell parameter c versus the concentration of Ca^{2+} in the solid solution for experiments with (1) 10 ppm Ca^{2+}, pH 6.6, and no flow; (2) 100 ppm Ca^{2+}, pH 6.6, and no flow; (3) and (7) 1000 ppm Ca^{2+}, pH 6.6, and no flow; (4) 10,000 ppm Ca^{2+}, pH 5.5 at 300 rpm; (5) 10,000 ppm Ca^{2+}, pH 5.5 at 600 rpm; (6) 10,000 ppm Ca^{2+}, pH 5.5, and no flow; (8) 10,000 ppm Ca^{2+}, pH 6.6, and no flow.

Figure 11 chart — Volume versus x. Labels: "pure CaCO₃", "6&7&8", "4&5", "2&3", "1", "pure FeCO₃". Y-axis: Volume (250, 300, 350, 400). X-axis: x (0, 0.2, 0.4, 0.6, 0.8, 1).
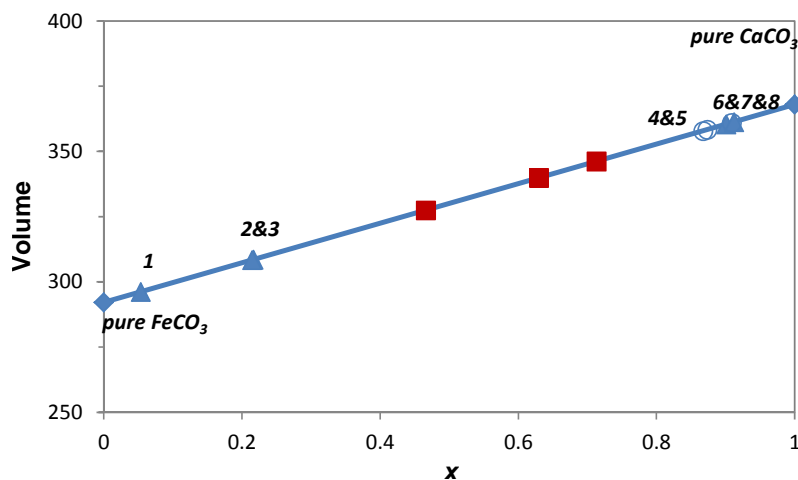
Figure 11: Unit cell volume versus concentration of Ca^{2+} in solid solution for experiments with (1) 10 ppm Ca^{2+}, pH 6.6, and no flow; (2) 100 ppm Ca^{2+}, pH 6.6, and no flow; (3) and (7) 1000 ppm Ca^{2+}, pH 6.6, and no flow; (4) 10,000 ppm Ca^{2+}, pH 5.5 at 300 rpm flow; (5) 10,000 ppm Ca^{2+}, pH 5.5 at 600 rpm flow; (6) 10,000 ppm Ca^{2+} , pH 5.5, and no flow; (8) 10,000 ppm Ca^{2+}, pH 6.6, and no flow.

Table 2

Composition of the solid solution.

Flow Condition	Initial Ca^{2+}/ppm	Weight Loss Corrosion mm/yr	Localized Corrosion mm/yr	Calculated x from EDS Spectra	Calculated x from XRD Data using "c"	Calculated x from XRD Data using "V"	Ca$_x$Fe$_y$CO$_3$ (x+y=1)
Previous Study							
Stagnant	10	0.6	-	0.045	0.05	0.05	Ca$_{0.05}$Fe$_{0.95}$CO$_3$
	100	NA	-	0.22	0.22	0.22	Ca$_{0.22}$Fe$_{0.78}$CO$_3$
	1,000	1.3	-	†	0.25	0.21	Ca$_{0.25}$Fe$_{0.75}$CO$_3$
				†	0.94	0.90	Ca$_{0.94}$Fe$_{0.06}$CO$_3$
	10,000	0.7	6.0	0.91	0.94	0.91	Ca$_{0.94}$Fe$_{0.06}$CO$_3$
Current Study							
Stagnant	10,000	0.8	8.5	0.96	0.91	0.91	Ca$_{0.91}$Fe$_{0.09}$CO$_3$
300 rpm	10,000	0.5	6.2	0.94	0.88	0.87	Ca$_{0.88}$Fe$_{0.12}$CO$_3$
600 rpm	10,000	1.2	-	0.91	0.88	0.87	Ca$_{0.88}$Fe$_{0.12}$CO$_3$

† As previously reported, the steel surface is covered with a bilayer at this Ca^{2+} concentration, so calculating the x value based on EDS data would not be representative.[1]

Analysis

Based on the results shown above, we are now in the position to try and answer the three questions posed at the beginning.

1. *Is it Cl⁻ or Ca^{2+} that leads to localized corrosion of mild steel in CO$_2$ solutions?* From Figure 6 it is apparent that in the experiment where there was no Ca^{2+} in the solution (Figure 6a) there was no localized corrosion. In the equivalent experiment that contained Ca^{2+},

localized corrosion was observed, suggesting that the cause of localized corrosion is related to the presence of Ca^{2+} rather than Cl^-.

2. *What is the effect of flow on the protectiveness of the precipitated $Fe_xCa_yCO_3$ layer?* Referring to Figure 1 it is seen that flow affects the general corrosion rates when at stagnant and low velocity a low corrosion rate is seen due to formation of a possible protective layer (see Figure 5), while at higher velocity a high corrosion rate is obtained. However, at stagnant and low velocity conditions localized corrosion is observed (see Figure 6) suggesting that only a partially protective layer was formed. There was no localized corrosion at high velocity when an unprotective layer formed.

3. *What is the exact composition of the $Fe_xCa_yCO_3$ layers precipitated on the mild steel surface and how is it related to corrosion?* The exact composition of the $Fe_xCa_yCO_3$ layers was reported in Table 2. In case of monolayer it seems that the higher mole fraction of Ca^{2+} could potentially lead to localized corrosion. However, it remains unclear why the condition with 600 rpm did not suffer any localized corrosion.

CONCLUSIONS

A mixed layer of $Ca_xFe_yCO_3$ ($x+y=1$) was detected on a steel surface exposed to a solution containing Ca^{2+} and aqueous CO_2, due to the isostructurality of $CaCO_3$ and $FeCO_3$. In some of these conditions (in the presence of high concentration $CaCl_2$) localized corrosion was observed. Additional experimentation showed that the effect of Ca^{2+} to be responsible for initiation of localized corrosion rather than the Cl^-. It was shown that flow affects the layer formation. The more agitated solution leads to a less protective $Ca_xFe_yCO_3$ layer. Using XRD data and EDS spectra, the mole fraction (x) of Ca^{2+} in $Ca_xFe_yCO_3$ ($x+y=1$) was independently calculated. When the mole fraction of Ca^{2+} in the $Ca_xFe_yCO_3$ ($x+y=1$) unit cell was close to one, the protectiveness of the layer was diminished.

ACKNOWLEDGMENTS

REFERENCES

1. S. N. Esmaeely, Y. Choi, D. Young, and S. Nešic, "Effect of Calcium on the Formation and Protectiveness of Iron Carbonate Layer in CO_2 Corrosion," *Corrosion Journal*, 69(2013), p. 912-920.

2. A. Dugstad, "Mechanism of Protective Film Formation during CO_2 Corrosion of Carbon Steel," paper no. 31 (Houston, TX: NACE, 1998).

3. J. K. Heuer, and J. F. Stubbins, "An XPS Characterization of $FeCO_3$ Films from CO_2 Corrosion," *Corrosion Science* 41(1999): p. 1231–1243.

4. M. B. Kermani and A. Morshed, "Carbon Dioxide Corrosion in Oil and Gas Production-A Compendium" *Corrosion* 59(2003): p. 659–683.

5. S. Nešić , and L. Lunde, "Carbon Dioxide Corrosion of Carbon Steel in Two-Phase Flow," *Corrosion* 50(1994): p. 717–727.

6. S. Nešić, "Carbon Dioxide Corrosion of Mild Steel," in *Uhlig's Corrosion Handbook*, 2011, pp. 229–245

7. C. A. Palacios, and J. R. Shadley, "Characteristics of Corrosion Scales on Steels in a CO_2-Saturated NaCl Brine," *Corrosion* 47(1991): p. 122–127.

8. S. Nešić, "Effects of Multiphase Flow on Internal CO_2 Corrosion of Mild Steel Pipelines," *Energy&Fuels* 26(2012): p. 4098–4111

9. R. Nyborg, and A. Dugstad, "Initiation and Growth of Mesa Corrosion Attack during CO_2 Corrosion of Carbon Steel," paper no. 29 (Houston, TX: NACE, 1998).

10. X. Jiang, Y. G. Zheng, D. R. Qu, and W. Ke, "Effect of Calcium Ions on Pitting Corrosion and Inhibition Performance in CO_2 Corrosion of N80 Steel," *Corrosion Science* 48(2006): p. 3091–3108.(6)

11. C. Q. Ren, X. Wang, L. Liu, H. E. Yang, and N. Xian, "Lab and Field Investigations on Localized Corrosion of Casing," *Materials and Corrosion* 63(2012): p. 168–172.

12. S. D. Zhu, J. F. Wei, Z. Q. Bai, G. S. Zhou, J. Miao, and R. Cai, " Failure Analysis of P110 Tubing String in the Ultra-deep Oil Well," *Engineering Failure Analysis* 18(2011): p. 950–962.

13. K. Gao, F. Yu, X. Pang, G. Zhang, L. Qiao, W. Chu, and M. Lu, "Mechanical Properties of CO_2 Corrosion Product Scales and their Relationship to Corrosion Rates," *Corrosion Science* 50(2008): p. 2796–2803.

14. ASTM Standard, "Standard Practice for Preparing, Cleaning, and Evaluating Corrosion Test," Reapproved, 1999.

15. S. Nešić, "Key Issues Related to Modeling of Internal Corrosion of Oil and Gas Pipelines – A Review," *Corrosion Science* 49(2007): p. 4308–4338

16. S. Nešić, M. Nordsveen, R. Nyborg, and A. Stangeland, "A Mechanistic Model for Carbon Dioxide Corrosion of Mild Steel in the Presence of Protective Iron Carbonate Films-Part 2: A numerical Experiment," *Corrosion Science* 59(2003): p. 489–497.

17. B. F. M. Pots and S. D. Kapusta, "Prediction of Corrosion Rates of the Main Corrosion Mechanisms in Upstream Applications," paper no. 05550 (Houston, TX: *NACE*, 2005).

18. W. Sun, S. Nešić, and R.C. Woollam, "The Effect of Temperature and Ionic Strength on Iron Carbonate ($FeCO_3$) Solubility Limit," *Corrosion Science* 51(2009): p. 1273–1276.

19. L. Plummer, E. Busenberg, *Geochimica et Cosmochimica Acta*, 46(1982), p.1011-1040.

20. "Mineralogy Database," 2012. [Online]. Available: http://webmineral.com/

21. A. R. West, *Solid state chemistry and its applications.* Aberdeen, Scotland: John Wiley & Sons, 1998, pp. 694.

22. P. M. Davidson, G. H. Symmes, B. A. Cohen, R. J. Reeder, and D. H. Lindsley, "Synthesis of the New Compound $CaFe(CO_3)_2$ and Experimental Constraints on the $(Ca,Fe)CO_3$ Join, "*Geochimica et Cosmochimica Acta,* 58(1994), p. 5105–5109.